Supporting Information for:

West African Monsoon dynamics inferred from abrupt fluctuations of Lake Mega-Chad.

Simon J. Armitage, Charlie S. Bristow, and Nick A. Drake

S1.0 Constraining lake level fluctuations in the Chad and Bodélé basins

The Palaeolake Mega-Chad basin is comprised of two separate but interlinked depressions (Figure 1c), termed the Chad and Bodélé basins. The northern (Bodélé) basin has a basal elevation of ~167 m, while the southern (Chad) basin has a basal elevation of ~276 m. These basins are separated by a watershed, whose lowest point, the Bahr el Ghazal (BEG) sill, has an elevation of 287 m. Below the level of the BEG sill, lake level information derived from one basin does not apply to the other basin, except that both lake surfaces must be below 287 m. Above 287 m, lakes in the Chad and Bodélé basins join to form a single large lake termed Lake Mega-Chad. Lake level information for Lake Mega-Chad applies to both basins. Because we used samples from both Chad and Bodélé to reconstruct the fluctuations of lakes in these basins, the two lake level histories are subtly different. Separate reconstructions of lake levels in the Chad and Bodélé basins are presented in Figure S1. It is important to note that the key fluctuations discussed in our paper (onset of humidity at ~15 ka, a Lake Mega-Chad highstand from 11.5-5 ka and an abrupt termination of the African Humid Period at 5 ka) are common to both records. After 5 ka, lowstands of Lake Chad are defined by samples from the Bodélé basin, and hence it is only possible to assert that the lake surface was below the elevation of the BEG sill, and at or above the present-day level at these times.

S1.1 Ages used to constrain fluctuations of Lake Mega-Chad

Sample details for all new and published (1-3) ages discussed in this study are given in Table S1. Figures S2-7 give locations for the new samples analysed in this study.

S2.0 Optically stimulated luminescence dating

Optically stimulated luminescence (OSL) dating is a radiometric dating technique which allows the determination of the time elapsed since a mineral grain was last exposed to sunlight. Where the mineral grains dated form part of a sediment, the OSL age is generally assumed to relate to the time at which that sediment was deposited (e.g. a sandy shoreline) or ceased to be active (e.g. a dune). The method has been successfully applied to a wide range of archaeological and Quaternary sediments (4-6). OSL dating is based upon the time dependant exposure of mineral grains (usually quartz or feldspar) to ionising radiation from naturally occurring radioisotopes within the sediment body (the ^{238}U, ^{235}U and ^{232}Th decay series and also ^{40}K) and also from cosmic rays. Ionising radiation causes electrons to become trapped at defects within the mineral's crystal lattice. Upon exposure to sunlight, electrons are released from their traps, resetting the trapped electron population to zero. Controlled exposure to light in the laboratory (optical stimulation) also causes trapped electrons to be released, and a proportion of these electrons dissipate energy as photons (luminescence). The intensity of the luminescence signal is proportional to the trapped electron population, which is in turn proportional to the total ionising radiation dose to which the mineral grain has been exposed since burial (palaeodose). Consequently, the equivalent dose (D_e), which is the laboratory estimate of the palaeodose, may be determined by measuring the OSL

intensity of a sample which has not been exposed to sunlight since burial. Since the ionising radiation flux (environmental dose rate, D_r) may usually be assumed to be constant, the burial age of the mineral grain may be calculated by dividing the equivalent dose by the environmental dose rate. The resulting OSL age is obtained in calendar years prior to the date of measurement. The datum for ages presented here is 2014. All measurements, analysis and interpretation of data necessary to generate OSL ages were performed by SJA.

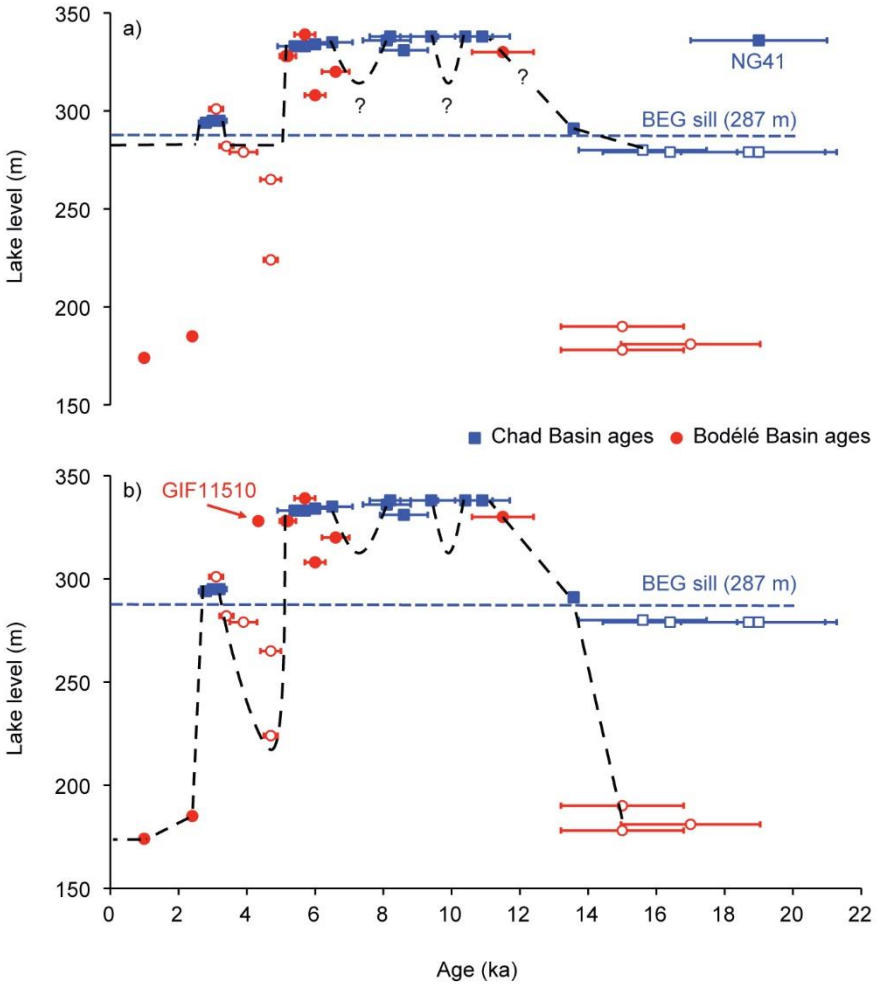

Figure S1. Separate lake level reconstructions (black dashed line) for a) the Chad Basin and b) the Bodélé basin. Blue symbols represent samples taken in the Chad basin, while red symbols represent samples taken in the Bodélé basin. Solid symbols represent shorelines, littoral molluscs or valley fills and therefore define contemporaneous lake level. Open symbols represent aeolian sediments, which were deposited above contemporaneous lake level, and therefore define the maximum lake level possible at that time. Samples taken from above the BEG sill constrain lake levels in both the Chad and Bodélé basins. Samples taken from below the BEG sill only constrain lake levels in that basin, though they do indicate that lake levels in both basins must have been below 287 m at that time. No absolute lake levels are available for the Lake Chad lowstands after 5 ka, though during these periods the lake level must have been below the BEG sill and at or above present day levels (~279 m). Consequently the lake level depicted in a) for the Lake Chad lowstands after 5 ka is illustrative rather than absolute. Samples NG41 and GIF11510 are shown on Figures S1a and S1b respectively, but were not included in the lake-level reconstruction (see Section 3 of the main text).

Table S1: Sample details for the ages used to constrain fluctuations of Lake Mega-Chad. In addition to ages presented in this study, published ages from a number of sources are included, and are acknowledged via a reference in the "Laboratory code" column. Samples are listed by type (aeolian sands or waterlain sediments) in chronological order. Laboratory codes with an asterisk indicate that the sample was excluded from the final lake level reconstruction. The reasons for rejecting these samples are discussed in the main text.

Region	**Location** (N°, E°)	**Age (ka)**	**Elevation (m)**	**Laboratory code**	**Method**	**Material**
Aeolian sands						
Madayi Island	13° 24' 21.4" 13° 48' 43.3"	19.0±2.3	279	NG35	OSL	Dune sand from Lake Chad island
Madayi Island	13° 24' 21.4" 13° 48' 43.3"	18.7±2.2	279	NG34	OSL	Dune sand from Lake Chad island
Bodélé	16° 42' 17.5" 17° 42' 57.1"	17.0±2.0	181	CH 51	OSL	Sand from barchan dune beneath diatomite
Zango 2 Island	13° 22' 05.9" 13° 50' 08.5"	16.4±2.0	279	NG36	OSL	Dune sand from Lake Chad island
Phulkime Island	13° 17' 14.7" 13° 52' 57.5"	15.6±1.9	280	NG33	OSL	Dune sand from Lake Chad island
Bodélé	16° 52' 48.5''18° 32' 38.2''	15.0±1.8	190	CH16	OSL	Sand from barchan dune beneath diatomite
Bodélé	16° 46' 45.6" 18° 17' 57.5"	15.0±1.8	178	CH22	OSL	Sand from barchan dune beneath diatomite
Erg du Djourab	17° 54' 22" 19° 05' 23"	4.7±0.2	224	BN197 (2)	OSL	Stabilised sand dune
Erg du Djourab	16° 23' 25" 18° 36' 59"	4.7±0.3	265	BN199 (2)	OSL	Stabilised sand dune
Erg du Djourab	15° 06' 50" 17° 42' 04"	3.9±0.4	279	BN200 (2)	OSL	Stabilised sand dune
Erg du Djourab	14° 50' 41" 17° 15' 28"	3.4±0.2	282	BN201 (2)	OSL	Stabilised sand dune
Erg du Djourab	13° 50' 31" 16° 28' 43"	3.1±0.2	301	BN202 (2)	OSL	Stabilised sand dune
Waterlain sediments (continued overleaf)						
Dalori Quarters IV	11° 46' 48.0" 13° 12' 42.7"	19.0±2.0	336	NG41*	OSL	Beach ridge sands
Monguno	12° 43' 13° 34'	13.7-13.4	291	SUERC-18367	^{14}C	Shells in sand and marl
Goz Kerki	15° 50' 17.2" 18° 42' 57.4"	11.5±0.9	330	CH74	OSL	Beach ridge sands
Ngomari	11° 45' 54.3" 13° 13' 57.8"	10.9±0.8	338	NG7	OSL	Fluvial sands
Ngomari	11° 45' 54.3" 13° 13' 57.8"	10.4±0.8	338	NG6	OSL	Fluvial sands
Kurimari II	11° 56' 24.8" 13° 01' 03.7"	9.4±0.9	338	NG11	OSL	Beach ridge sands
Magumeri	12° 08' 00.9" 12° 49' 05.6"	8.6±0.7	331	NG12	OSL	Beach ridge fluvial sediments
Ngomari	11° 45' 54.3" 13° 13' 57.8"	8.2±0.6	338	NG8	OSL	Fluvial sands
Dalori Quarters III	11° 46' 55.0" 13° 12' 45.9"	8.1±0.7	336	NG40	OSL	Beach ridge sands
Goz Kerki	15° 51' 30.8" 18° 43' 18.8"	6.6±0.4	320	CH73	OSL	Beach ridge sands
Dalori Quarters I	11° 46' 32.0" 13° 13' 19.5"	6.5±0.6	335	NG38	OSL	Beach ridge sands
Dalori Quarters II	11° 47' 01.5" 13° 12' 50.9"	6.0±0.6	334	NG39	OSL	Beach ridge sands
Angamma	17° 34' 00.0" 17° 49' 51.4"	6.0±0.3	308	CH46	OSL	Beach ridge sands
Kurimari I	11° 55' 33.9" 13° 02' 11.5	5.7±0.4	333	NG10	OSL	Beach ridge sands

Region	Location (Nº, Eº)	Age (ka)	Elevation (m)	Laboratory code	Method	Material
Waterlain sediments (continued from previous page)						
Angamma	17º 35’ 14.2” 17º 39’ 41.5”	5.7±0.3	339	CH44	OSL	Beach ridge sands with pebbles
Kurimari I	11° 55’ 32.7” 13° 02’ 13.4”	5.4±0.5	333	NG9	OSL	Beach ridge sands
Goz Kerki	16º 24’ 18º 58’	5.31-4.98	328	GIF11511 (1)	^{14}C	Shells
Goz Kerki	16º 24’ 18º 58’	5.44-4.97	328	GIF11512 (1)	^{14}C	Shells
Goz Kerki	16º 24’ 18º 58’	4.52-4.16	328	GIF11510 (1)*	^{14}C	Shells
Ngelewa I	13° 04’ 45.7” 13° 36’ 42.9”	3.2±0.2	295	NG31	OSL	Beach ridge sands
Ngelewa I	13° 04’ 45.7” 13° 36’ 42.9”	3.0±0.2	295	NG32	OSL	Beach ridge sands
Ngelewa Ridge	13° 00’ 02.6” 13° 38’55.5”	2.8±0.2	294	NG29	OSL	Beach ridge sands
Bahr el Ghazal	16º 41’ 03.2” 18º 01’ 42.0”	2.4±0.1	185	CH62 (3)	OSL	Sand overlain by 30 cm of clay
Bodélé	16˚ 47’ 17.6” 17˚ 50’13.2”	1.06-0.93	174	SUERC-18366	^{14}C	Shells in diatomite.

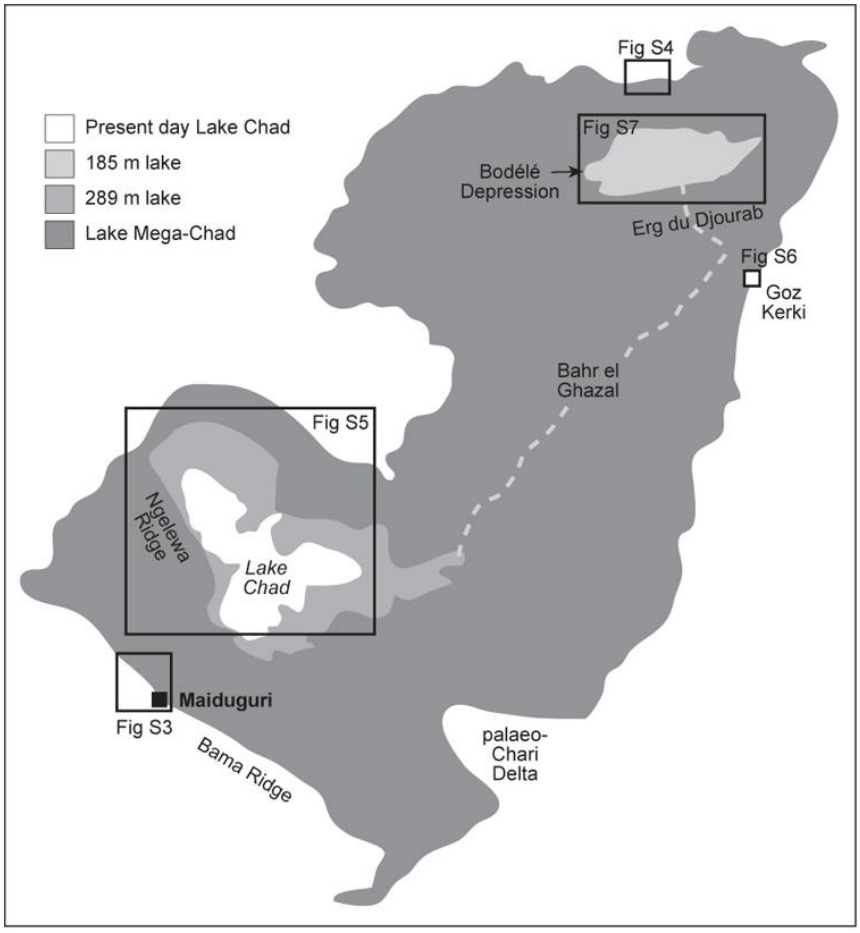

Figure S2. Lake Mega-Chad, showing the location of areas illustrated in Figures S3-7.

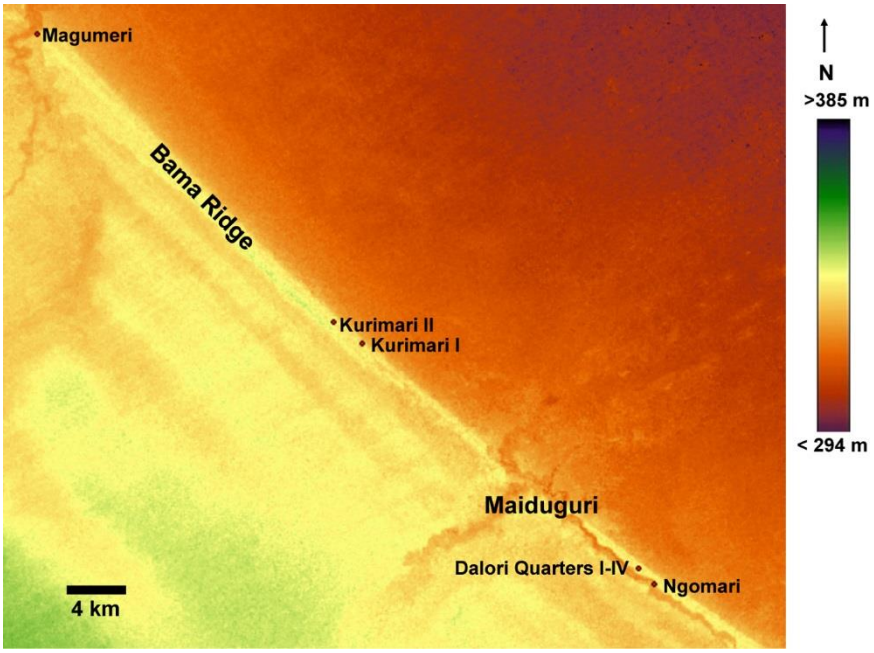

Figure S3. Digital elevation model (DEM) for the Bama Ridge showing sample locations and features mentioned in the text.

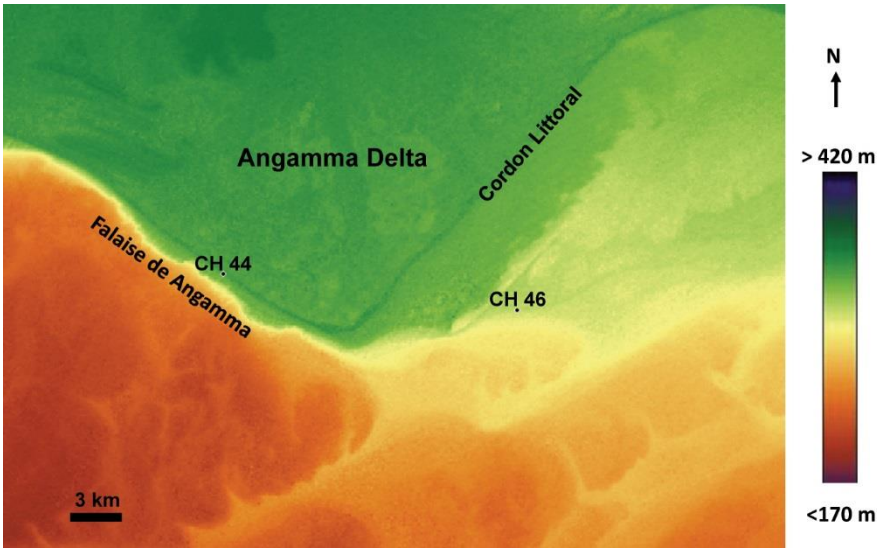

Figure S4. Digital elevation model (DEM) of the Angamma delta showing sample locations and features mentioned in the text.

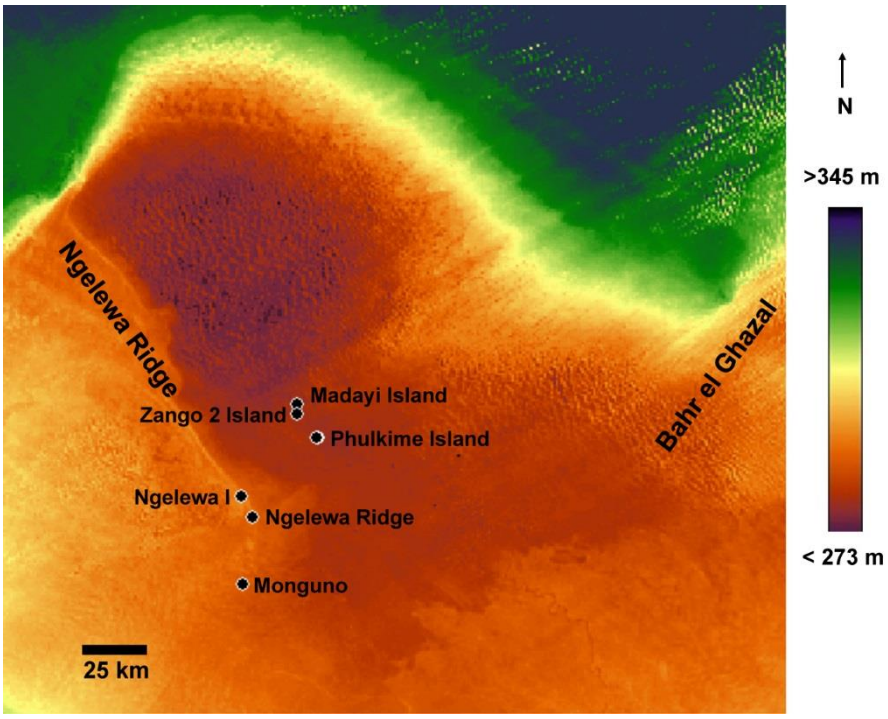

Figure S5. Digital elevation model (DEM) of Lake Chad showing sample locations and features mentioned in the text.

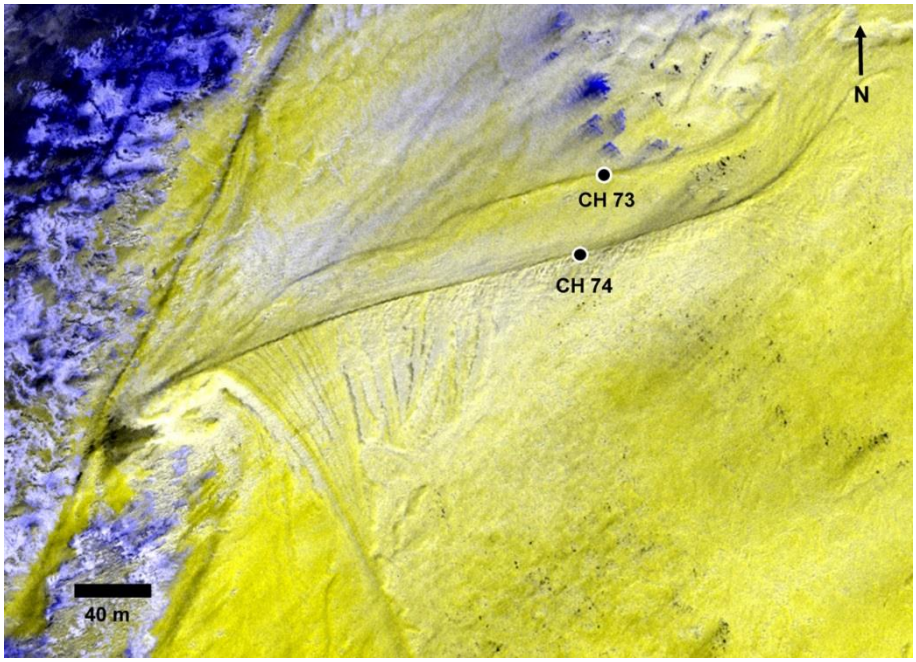

Figure S6. Landsat Thematic Mapper false colour composite (RGB 742) of the Goz Kerki sand spit showing beach ridge sample locations.

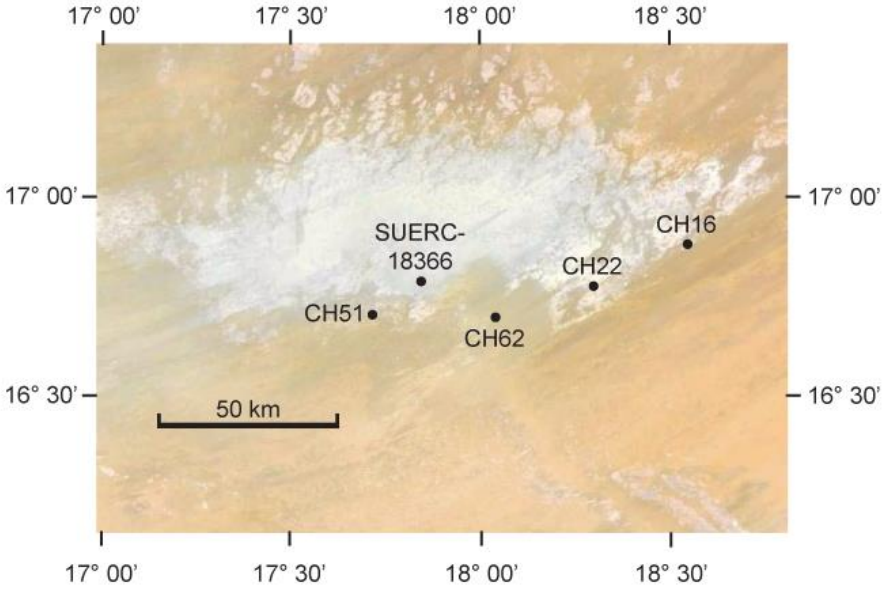

Figure S7. Satellite image of the Bodélé depression showing the locations of samples and of deflating diatomite (light grey).

S2.1 OSL sample collection and preparation

Samples were collected from cleaned sections either in opaque plastic tubes hammered into the section, or in opaque plastic bags. In the latter case, the sampled unit was shielded from sunlight by black tarpaulin. In the laboratory, samples were processed under orange light. A sub-sample of each sample was retained for dose rate measurement.

Quartz was extracted from each sample using standard laboratory techniques. Briefly, samples were wet-sieved to 212-180 µm (sample codes starting with the letters "NG") or 180-150 µm (sample codes starting with the letters "CH"), and carbonates and organic matter were subsequently removed using 1M HCl and H_2O_2 respectively. The samples were then re-sieved to 180 or 150 µm, and quartz was extracted from the retained fraction using density separations at 2.75 and 2.62 g/cm^3 and a subsequent HF acid etch (23M HF for 60 min followed by a 24 hour immersion in 10M HCl). Finally, etched samples were again re-sieved to 180 or 150 µm, to remove partially dissolved grains, and stored in opaque containers prior to measurement.

S2.2 Luminescence measurements

All measurements presented in this study were carried out using a Risø TL/OSL-DA-15 automated dating system (7). Optical stimulation was carried out using a blue (470 nm) light emitting diode (LED) array, while infra-red stimulation was carried out using an infra-red diode array. These sources have nominal power densities of 33 and 132 mW/cm^2 respectively (7). Irradiation was carried out using a 40 mCi ^{90}Sr/^{90}Y β-source calibrated relative to the National Physical Laboratory, Teddington ^{60}Co γ-source (8). OSL was detected using an Electron Tubes Ltd 9235QB15 photomultiplier tube having first passed through 7.5 mm of Hoya U-340 filter.

The single-aliquot regenerative-dose (SAR) method (9, 10) was used to determine the equivalent dose (D_e). An infra-red wash (40 s at room temperature) was used prior to all OSL measurements (11), and OSL decays were measured over 40 s (Figure S8a). The luminescence intensity used for D_e determination was that from the first 10.6 mJ/cm^2 of stimulation, with a background derived from the last 132 mJ/cm^2 of stimulation subtracted. A 5 Gy test dose was used for all samples. Aliquots were heated at 5 ºC/s during all heating steps, and a 10 second pause at 125 ºC prior to optical stimulation was used to allow for the lag in temperature between the thermocouple and sample. Eight commonly adopted preheating regimes were used for all samples (Figure S9), with three aliquots being measured using each preheat regime. A wide range of PH1 temperatures were used to check for the presence of a thermally-transferred OSL signal at higher temperatures, however no trend in D_e with PH1 temperature was observed (Figure S9). Growth curves were fitted using a saturating-exponential-plus-linear function (Figure S8b). Curve fitting and equivalent dose determination were performed using version 3.24 of the Luminescence Analyst software (12). Uncertainties were estimated using the "Monte Carlo repeats" option in Analyst (1,000 iterations) and incorporate an instrument specific 1.5% error per OSL measurement.

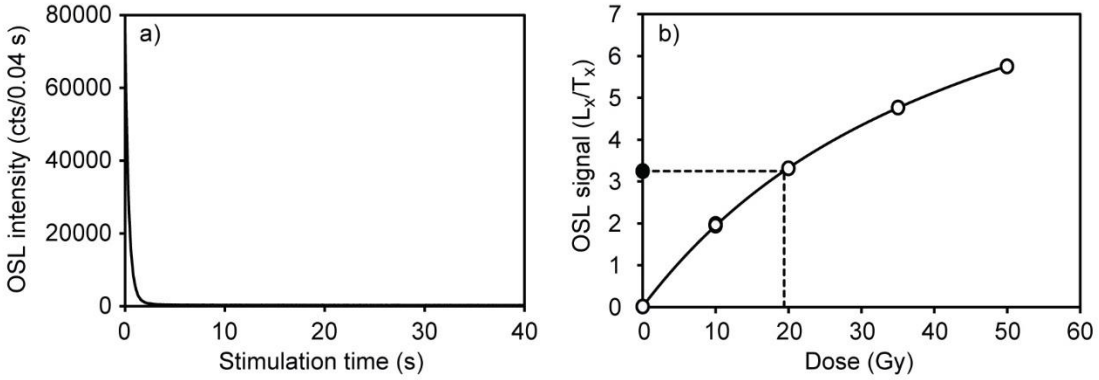

Figure S8. Typical OSL data a) natural decay curve for sample NG38, and b) dose response curve for the same aliquot. The recycling ratio and IR-depletion ratio tests were performed using a 10 Gy regeneration point, but all three points overlie each other.

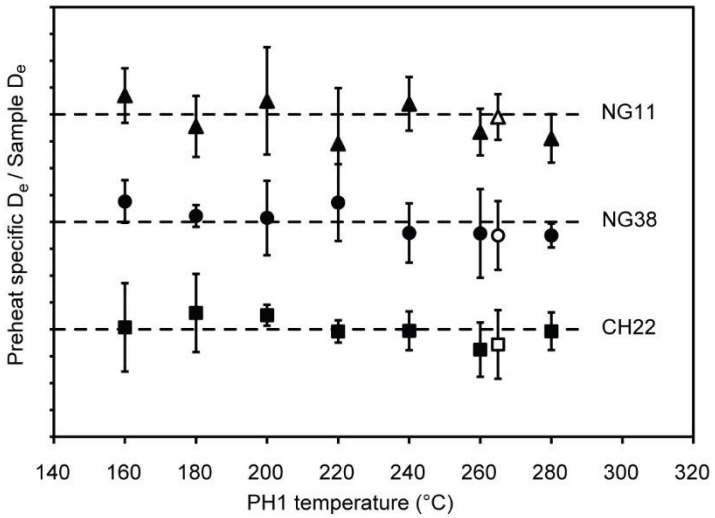

Figure S9. Equivalent dose dependence upon PH1 temperature for samples CH22 (3.27 ± 0.10 Gy), NG38 (19.1 ± 0.6 Gy) and NG11 (27.7 ± 1.0 Gy). Each point is the mean of three aliquots. Solid markers indicate data where a 160 °C cut-heat was used for PH2. The open markers represent data where a 260°C PH1 and 220 °C PH2, both held for 10 s, were used. These data have been offset by 5 °C on the x-axis for clarity. Dashed lines represent a preheat specific De/Sample De ratio of 1, and the Y-axis tick marks are spaced at 0.05 (5%) intervals.

S2.3 Equivalent dose determination

Prior to calculating an equivalent dose for each sample, the reliability of data from each individual aliquot was assessed. Recycling ratios were calculated to monitor the performance of the SAR procedure (10) while sample purity was assessed using the IR depletion ratio method (13). Aliquots not yielding recycling or IR depletion ratios consistent with unity were rejected. In addition, aliquots exhibiting high recuperation (i.e. the sensitivity-corrected luminescence intensity for the 0 Gy regeneration point is greater than 5 % of the sensitivity-corrected natural luminescence intensity) were rejected. Approximately 10 % of aliquots were rejected (~2 aliquots per sample), the vast majority due to failing the recycling ratio test. Sample equivalent doses were calculated by applying the Central Age Model (CAM, 9) to aliquots which passed the above rejection criteria.

S2.4 Environmental dose rate calculations

For the majority of samples reported in this study, the environmental dose rate may be assumed to be constant over time. However, the dunes in the Bodélé Depression (CH16, CH22 and CH51) and Lake Chad (NG33-36) were submerged for much of the time since deposition, causing dose rates to vary. The procedure used to calculate dose rates and ages for these samples is described in Section S2.6. Dose rates for all other samples were calculated using the more conventional procedure described below.

For HF acid etched sand-sized quartz grains, the environmental dose rate consists of external beta, gamma and cosmic ray components. Beta and gamma dose rates were calculated from the radioisotope concentration of the host sediments using standard conversion factors (14). Radioisotope concentrations were determined using ICP-MS (U and Th) and ICP-AES (K). Secular equilibrium in the uranium and thorium decay series was assumed. Dose rates were corrected for the effects of grain size (15), HF etching and water content (16). The assumed water content of 5±5% encompasses the full range of likely burial conditions. Cosmic ray dose rates were calculated using site location (latitude and longitude), elevation and present day burial depths, assuming an overburden density of 1.85 g/cm^3 (17, 18). Environmental dose rates are presented in Table S2.

Table S2. Sample depth, water content and dose rates. Depths are below present day ground surface.

Sample name	Sample depth (m)	Moisture content (%)	Dose rate (Gy/ka)			Total dose rate, Dr (Gy/ka)
			Beta	Gamma	Cosmic	
NG41	2.3±0.2	5±5	1.76±0.20	0.97±0.08	0.15±0.00	2.88±0.21
CH74	0.5±0.1	5±5	0.43±0.04	0.27±0.02	0.20±0.01	0.90±0.05
NG7	7.5±0.5	5±5	1.68±0.18	1.11±0.09	0.09±0.00	2.88±0.20
NG6	8.5±0.5	5±5	2.41±0.25	1.63±0.12	0.08±0.00	4.12±0.28
NG11	5.0±0.2	5±5	1.94±0.23	0.89±0.08	0.11±0.00	2.94±0.25
NG12	5.0±0.2	5±5	1.64±0.19	0.89±0.07	0.11±0.00	2.64±0.20
NG8	3.5±0.5	5±5	2.10±0.20	1.69±0.13	0.13±0.01	3.93±0.24
NG40	1.7±0.2	5±5	2.15±0.16	0.94±0.09	0.16±0.00	3.25±0.28
CH73	0.5±0.1	5±5	0.43±0.04	0.33±0.02	0.20±0.01	0.96±0.05
NG38	1.8±0.2	5±5	1.89±0.22	0.91±0.08	0.16±0.00	2.97±0.24
CH46	0.5±0.1	5±5	0.38±0.03	0.30±0.02	0.20±0.01	0.89±0.04
NG39	2.2±0.2	5±5	2.30±0.28	0.99±0.10	0.15±0.00	3.45±0.30
CH44	0.5±0.1	5±5	0.19±0.01	0.20±0.02	0.20±0.01	0.59±0.02
NG10	3.4±0.2	5±5	1.56±0.14	1.37±0.11	0.13±0.00	3.06±0.18
NG9	3.5±0.5	5±5	2.06±0.24	0.97±0.09	0.13±0.01	3.16±0.26
NG31	2.95±0.2	5±5	0.30±0.03	0.26±0.02	0.14±0.00	0.69±0.03
NG32	1.75±0.2	5±5	0.08±0.01	0.14±0.01	0.16±0.00	0.39±0.02
NG29	2.25±0.2	5±5	0.19±0.02	0.14±0.01	0.15±0.00	0.48±0.02
CH62	0.5±0.1	5±5	0.17±0.02	0.12±0.01	0.20±0.01	0.50±0.02

S2.5 Age calculation

Ages for samples other than the dunes in the Bodélé Depression (CH16, CH22 and CH51) and Lake Chad (NG33-36) were calculated using Eq.1.

Equation 1: $$Age = D_e/D_r$$

Where D_e is the equivalent dose determined using the CAM and D_r is the environmental dose rate. Equivalent doses, environmental dose rates and ages are presented in Table S3.

Table S3. Sample equivalent doses, environmental dose rates and ages. Dose rates and age calculations for samples where the total dose rate is listed as "variable" are described in Section S2.6, with numerical data being provided in Table S4.

Sample name	Number of aliquots	Equivalent dose, D_e (Gy)	Total dose rate, Dr (Gy/ka)	Age (ka)
NG35	17	5.25±0.24	Variable	19.0±2.3
NG41	19	54.5±4.1	2.88±0.21	19.0±2.0
NG34	17	5.60±0.23	Variable	18.7±2.2
CH51	20	4.10±0.14	Variable	17.0±2.0
NG36	15	3.63±0.18	Variable	16.4±2.0
NG33	17	6.74±0.27	Variable	15.6±1.9
CH16	19	3.40±0.14	Variable	15.0±1.8
CH22	20	3.27±0.10	Variable	15.0±1.8
CH74	20	10.3±0.6	0.90±0.05	11.5±0.9
NG7	17	31.4±0.7	2.88±0.20	10.9±0.8
NG6	21	42.8±1.5	4.12±0.28	10.4±0.8
NG11	20	27.7±1.0	2.94±0.25	9.4±0.9
NG12	19	22.8±0.8	2.64±0.20	8.6±0.7
NG8	20	32.3±1.2	3.93±0.24	8.2±0.6
NG40	20	26.4±0.9	3.25±0.28	8.1±0.7
CH73	22	6.33±0.24	0.96±0.05	6.6±0.4
NG38	19	19.1±0.6	2.97±0.24	6.5±0.6
CH46	21	5.30±0.17	0.89±0.04	6.0±0.3
NG39	17	20.6±1.0	3.45±0.30	6.0±0.6
CH44	18	3.37±0.16	0.59±0.02	5.7±0.3
NG10	19	17.4±0.7	3.06±0.18	5.7±0.4
NG9	19	17.2±0.7	3.16±0.26	5.4±0.5
NG31	18	2.20±0.10	0.69±0.03	3.2±0.2
NG32	19	1.16±0.06	0.39±0.02	3.0±0.2
NG29	19	1.32±0.05	0.48±0.02	2.8±0.2
CH62	22	1.22±0.04	0.50±0.02	2.4±0.1

S2.6 Age calculations for the Bodélé Depression and Lake Chad dunes

The dunes in the Bodélé Depression (CH16, CH22 and CH51) and Lake Chad (NG33-36) were submerged for much of the time since deposition, leading to time dependent changes in the environmental dose rate. These changes derive from two causes: a) variations in the cosmic ray dose rate due to changes in the depth of overlying water (up to 150 m in the Bodélé Depression) and b) variations in beta and gamma dose rates due to changes in the water content of the sediment itself. These variations necessitated an unconventional approach to calculating the depositional age of the samples. Firstly, the total radiation dose to which the sample had been exposed in the last 15 ka (before which the dunes were assumed to be subaerially exposed and dry) was calculated. Secondly, a modified age equation was used to calculate the age of each sample.

S2.6a Cosmic dose rates

The cosmic ray dose rate is controlled primarily by the sample depth and overburden density i.e. the mass of absorber overlying the sample (17, 18). Consequently, changes in lake level change the mass of absorber overlying the sample, and hence the cosmic ray dose rate.

To account for these changes, cosmic ray dose rates for the Bodélé Depression and Lake Chad dune samples were calculated in 500 year time slices for the last 15 ka, and summed. This approach allows calculation of the total cosmic ray dose experienced by each sample from the start of the African Humid Period (c.15 ka, 19) to the present day. It assumes that the samples were not submerged prior to 15 ka, and was performed

using each of three lake-level scenarios: a) the "gradual rise" scenario; b) the "early rise" scenario, and c) the "late rise" scenario. These scenarios differ in the timing and pattern of lake level rise between 15 and 11.5 ka, and were used to test the sensitivity of the calculation to these parameters, since little evidence is available for exact lake levels prior to c. 11.5 ka. The application of these scenarios to the Chad Basin is described first. The "gradual rise" scenario assumes that lake levels rose at a constant rate, starting with an empty Chad Basin prior to 15 ka and reaching the lake full level (330 m) at 11.5 ka (the age of the 330 m beach ridge at Goz Kerki, sample CH74). The "early rise" scenario assumes that from an empty Chad Basin, lake levels instantly rose to 330 m at 15 ka. This scenario is intended to replicate an abrupt onset of the African Humid Period (19) and represents the wettest conditions which the samples are likely to have experienced. The "late rise" scenario assumes that the Chad Basin remains dry until 11.5 ka, after which lake levels instantly rose to 330 m. This scenario represents the driest conditions which the samples are likely to have experienced. The "early rise" and "late rise" scenarios are readily applicable to the Bodélé basin, though the water depths here are ~100 m greater than in the Chad Basin. However, the "gradual rise" scenario as applied to the Bodélé basin envisages the altitude of the lake surface tracking that in the Chad Basin. For the 15-14.5 ka time slice this is probably inappropriate. However, after 14.5 ka the lake in the Chad Basin exceeds the level of the BEG sill, connecting the two basins to form a single water body. It is probable that none of these scenarios accurately reflect the lake level history between 15 and 11.5 ka. However, they do allow the calculation of cosmic ray dose rates for the most extreme ("early rise" and "late rise") and more realistic ("gradual rise") lake level histories which are consistent with our understanding of the pre-Holocene fluctuations of Lake Chad.

After 11.5 ka, all three scenarios assume the same lake level fluctuations. The situation for the Chad Basin is described first. From 11.5-5.5 ka lake levels remain constant at 330 m. Between 5.5 and 5 ka the lake level falls to 290 m (below the BEG sill, thereby allowing the deposition of the aeolian sands in the Erg du Djourab (2). Between 5 and 3 ka, lake levels remain constant at 290 m, and then rise again to 295 m (the elevation of the Ngelewa ridge) at 3 ka. Thereafter, lake levels fall at a constant rate, reaching the present day level of 280 m at 1 ka. Prior to 5 ka lake levels in the Bodélé basin were assumed to be identical to those in the Chad basin. Between 5 and 3 ka a lake level of 270 m (the mean level of the Erg du Djourab aeolian sand samples, 2) was assumed in the Bodélé basin. After the highstand which emplaced the Ngelewa ridge, Bodélé basin lake levels fell to 185 m at 2.5 ka (the age and altitude of sample CH62, sand underlying delta muds in the Bahr el Ghazal), and to 180 m (dry basin conditions) at 1 ka. This approach yielded a total cosmic ray dose over the last 15 ka for each sample and each lake level scenario (Table S4, $D_{cos\ variable}$).

S2.6b Beta and gamma dose rates

Water in the interstices between mineral grains absorbs a proportion of the ionising radiation dose which would otherwise have been absorbed by the mineral grains themselves (16). Consequently, dry beta and gamma dose rates, calculated from the radioisotope concentration of the sample, must be corrected according to the sample's water content. The beta and gamma doses for these samples were calculated in 500 year time slices for the last 15 ka, and summed. For the purposes of this calculation, samples were assumed to be either dry (above the water table) or saturated (below the water table), with a water content of 5±5% being assumed for the former, and 37±5% for the

latter (20). This calculation was performed for each of the lake level scenarios used to calculate total cosmic ray doses.

Table S4. Dosimetry data for the Bodélé Depression and Lake Chad dune samples. GR denotes the "gradual rise" scenario, LR (W) denotes the "late rise, wet" scenario, LR (D) denotes the "late rise, dry" scenario and ER denotes the "early rise" scenario. $D_{cos\ variable}$ is the total cosmic ray dose for the sample from 15 ka to the present day. $D_{ß+\gamma\ variable}$ is the total beta and gamma dose for the sample from 15 ka to the present. D_r is the dose rate which pertained prior to 15 ka, and D_e is the equivalent dose.

Sample name	Scenario	$D_{cos\ variable}$ (Gy)	$D_{ß+\gamma\ variable}$ (Gy)	D_r (Gy/ka)	D_e (Gy)	Age (ka)
NG33	GR	0.86	5.50	0.66	6.74	15.6
	LR (W)	1.25	5.50			15.0
	LR (D)[1]	1.23	5.29			14.3
	ER	0.73	5.50			15.8
NG34	GR	0.89	3.05	0.45	5.60	18.7
	LR (W)	1.30	3.05			17.8
	LR (D)	1.30	3.30			17.3
	ER	0.76	3.05			19.0
NG35	GR	0.73	2.90	0.40	5.25	19.0
	LR (W)	1.05	2.90			18.3
	LR (D)	1.05	3.15			17.7
	ER	0.63	2.90			19.3
NG36	GR	0.82	2.30	0.37	3.63	16.4
	LR (W)	1.20	2.30			15.3
	LR (D)[1]	1.18	2.28			14.4
	ER	0.71	2.30			16.7
CH16	GR	0.55	2.85	0.45	3.40	15.0
	LR (W)[1]	0.84	2.48			13.2
	LR (D)[1]	0.84	2.58			13.0
	ER	0.55	2.85			15.0
CH22	GR	0.51	2.75	0.44	3.27	15.0
	LR (W)[1]	0.79	2.39			13.2
	LR (D)[1]	0.79	2.48			13.0
	ER	0.50	2.75			15.0
CH51	GR	0.52	2.71	0.44	4.10	17.0
	LR (W)	1.21	2.65			15.7
	LR (D)	1.21	2.87			15.1
	ER	0.52	2.71			17.0

[1] $D_{cos\ variable}$ and $D_{ß+\gamma\ variable}$ for these samples were calculated for time periods shorter than 15 ka.

The application of these scenarios to the Chad Basin is described first. In the "gradual rise" and "early rise" scenarios, sediments were assumed to be below the water table from 15 ka to the present day (the Chad Basin samples are currently below the water table). In the "late rise" scenario, two plausible water content scenarios are envisaged.

Firstly, sediments may be above the water table until 11.5 ka, and then below the water table from 11.5 ka to the present day. Secondly, sediments may be below the water table from 15 ka to the present day. These two water content scenarios are referred to as the "late rise, dry" and "late rise, wet" scenarios respectively. In the Bodélé Depression, the same water content scenarios were applied, except that samples were assumed to be above the water table from 1 ka (the age radiocarbon date for an articulated freshwater bivalve shell buried in diatomite) to the present day.

This approach yielded a total beta and gamma dose over the last 15 ka for each sample and each lake level scenario (Table S4, $D_{ß+\gamma\ variable}$).

S2.6c Age calculation

Ages (ka) for the Bodélé Depression and Lake Chad dunes were calculated using Eq.2.

Equation 2. $$Age = ((D_e - D_{variable})/D_r) + 15$$

Where D_e is the equivalent dose (Gy), $D_{variable}$ is the sum of the beta, gamma ($D_{ß+\gamma\ variable}$) and cosmic doses ($D_{cos\ variable}$) absorbed by the sample over the last 15 ka (Gy), and D_r is the dose rate which pertained prior to 15 ka (Gy/ka). D_r was calculated using the method outlined in Section S2.4, assuming present day burial depth and a water content of 5±5%. Where this calculation yielded a sample age less than 15 ka, $D_{variable}$ was recalculated to provide the summed doses absorbed by the sample over the last 14 ka, and 14 ka (as opposed to 15 ka in Eq.2) added to the result. Dosimetry data and ages are presented in Table S3.

In all cases, the "late rise, dry" scenario yielded the oldest age whereas the "early rise" scenario yielded the youngest age, with the discrepancy between these ages for any given sample ranging from 1.5-2.3 ka. For the purposes of constraining the onset of lake-level rise, the ages determined using the "gradual rise" scenario has been used. These age estimates were preferred since a gradual rise in lake levels is considered to be more likely than very rapid lake level rises at either 15 or 11.5 ka, and is supported by the ages (12.9-11.5 ka) from the Komadugu palaeofloodplain (21). In practice, since the cosmic ray dose rate falls to very low levels with greater than 15 m submersion, the "gradual rise" and "late rise" scenarios yield very similar ages. Conversely, the "late rise, dry" ages are 11.7±3.5% lower than the preferred "gradual rise" ages. The "late rise, dry" scenario represents the driest conditions which are consistent with other data constraining pre-Holocene fluctuations of Lake Chad. Consequently, a plausible maximum uncertainty term on the "gradual rise" age is one which overlaps the "late rise, dry" age. For this reason, the ages for the Bodélé Depression and Lake Chad dunes have been assigned a 12% uncertainty.

S3.0 Radiocarbon dating

Table S1 contains the new (SUERC-18366/18367) and published (1) radiocarbon dates from Lake Mega-Chad which were used in this study. We have only used published ages obtained for macrofossils from shorelines, and ignored ages from archaeological sites which do not provide direct control on lake levels. Dates which have not had a ^{13}C correction applied were also excluded from consideration. The two new dates presented here are from the Bodélé Depression in Chad (SUERC-18366) and from near Monguno in Nigeria (SUERC-18367). The Bodélé Depression sample consists of in-situ bivalves from the lake bed sediments in the Bodélé Depression (Figure S10). Samples were collected by hand from the surface of a thin diatomite bed. Two of the bivalves in the centre of the picture, which were collected, are still articulated and partly buried in the lake sediments. This indicates that these bivalves are in-situ and have therefore not been deflated nor subject to any transport because they are still in life position within the lake sediments. The surrounding bivalves have been recently deflated from the same sediments but were not included in the sample for dating. The shells on the surface are in pristine condition, thus it is thought that they were recently exhumed from the lake sediments that were deposited during the final lake phase in the Bodélé Depression. The shells provided a radiocarbon age of 1061± 37 years (1.06-0.93 cal. ka BP), and represent the most recent dated occurrence of perennial standing water in the Bodélé Basin.

Figure S10. In-situ, articulated bivalves in the Bodélé Basin, dated as sample SUERC-18366. The two pairs of bivalve shells above the pen are preserved in life position within lake bed diatomite and were selected for radiocarbon dating.

The Monguno molluscs from northeast Nigeria, close to the shore of Lake Chad, were collected in 1959 by Sparks (22) and subsequently stored in the Sedgewick Museum, Cambridge. The shells were found at an elevation of 291 m, 8 miles south of Mongonu, at a site close the Ngelewa Ridge. The molluscs were found in a pit that was dug for a soil survey (Figure S11). The base of the pit consists of aeolian sand with fossil grass fragments that suggest stabilization after deposition. Above this is a thick layer of sand and marl containing abundant freshwater molluscs. It is these shells that were sampled and subsequently produced a conventional radiocarbon age of 11725 ± 39 years (13.7-13.4 cal. ka BP). We interpret the Monguno sediments as indicating initially arid conditions, followed by perennial freshwater lake conditions dated to 13.7-13.4 cal. ka BP. The dated molluscs are overlain by aeolian sands, indicative of a subsequent lake desiccation. The section is capped by black clay that could either be a soil or a lake sediment deposited in a further brief expansion of Lake Chad. We interpret the dated molluscs as representing the first expansion of Lake Chad following late glacial aridity, and note that the age estimate for this event is consistent with the first post-LGM freshening of the Gulf of Guinea (23). Aeolian sands overlying the mollusc rich sediments are interpreted as a desiccation event. These sands may have been emplaced during the drying observed in numerous records during at ~12 ka, or in the desiccation event after 5 ka. This might correlate with the dunes of the Lantewa dunefield in northeast Nigeria, which have been dated to between 6.98 ± 0.45 and 0.17 ±0.03 ka (24).

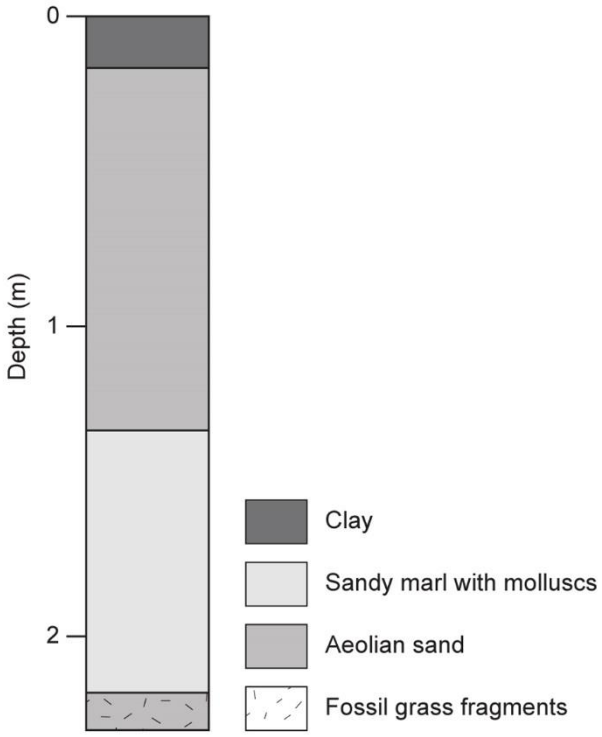

Figure S11. Sketch section of the site where the molluscs from the Sedgwick Museum were collected.

S4 OSL sample descriptions and interpretation

S4.0 Sand dunes

The dunes sampled and dated in this study are all examples of quartz rich sand dunes. Where possible the samples were collected from the downwind margin of stabilised or semi-stabilised dunes, so that the ages derived from the dune sediments may be interpreted to represent the most recent dune activity prior to stabilisation and burial of the preserved dune sands. In addition to the samples collected for this study we have included aeolian dune dates from the Erg du Djourab (2).

S4.1 Dune islands in Lake Chad

Lake Chad is dotted with elongated islands that trend NW to SE (Figure S12). These islands are interpreted to be transverse dunes that have been drowned by the rising lake waters and exposed recently as the lake waters fell (25). OSL dating of the dune islands was undertaken to determine when the dunes were last active, and by inference to constrain when lake waters flooded the dunes. Three dune islands in the Nigerian sector of Lake Chad were sampled using a hand auger (Figure S12). Sample NG33 is from a depth of 1.6 m in very fine grained pale buff coloured sands at Phulkime Island. Samples NG34 and 35 are fine and very fine grained pale buff coloured sands from Madayi Island. At Madayi, the borehole started in grey oxidised sands and passed down into orange iron stained sands at a depth of 1 m. Pale buff sands return at a depth of 1.5 m and continue to the bottom of the borehole at 3.45 m. Two samples were collected, NG34 at a depth of 2.3 m and NG35 at a depth of 3.25 m. At Zango 2 Island we collected one sample (NG36) from a depth of 2 m in pale buff coloured fine grained sand.

The OSL age for sample NG33 from Phulkime Island is 15.6 ± 1.9 ka, for NG34 and 35 at Madayi Island is 18.7 ± 2.2 ka and 19.0 ± 2.3 ka respectively, for NG36 from

Zango 2, 16.4 ± 2.0 ka. These central ages span four thousand years from 19.0 ± 2.3 to 15.6 ± 1.9 ka. This age range corresponds with the timing of the deglaciation between 20 and 15 ka (26). We infer that the dunes were active during the last glacial maximum but stabilised shortly thereafter during the deglaciation, corresponding with a shift from arid to more humid conditions. It is possible that the dunes were stabilised by vegetation prior to the lake transgression, so these ages may predate the lake level rise that flooded the dunes.

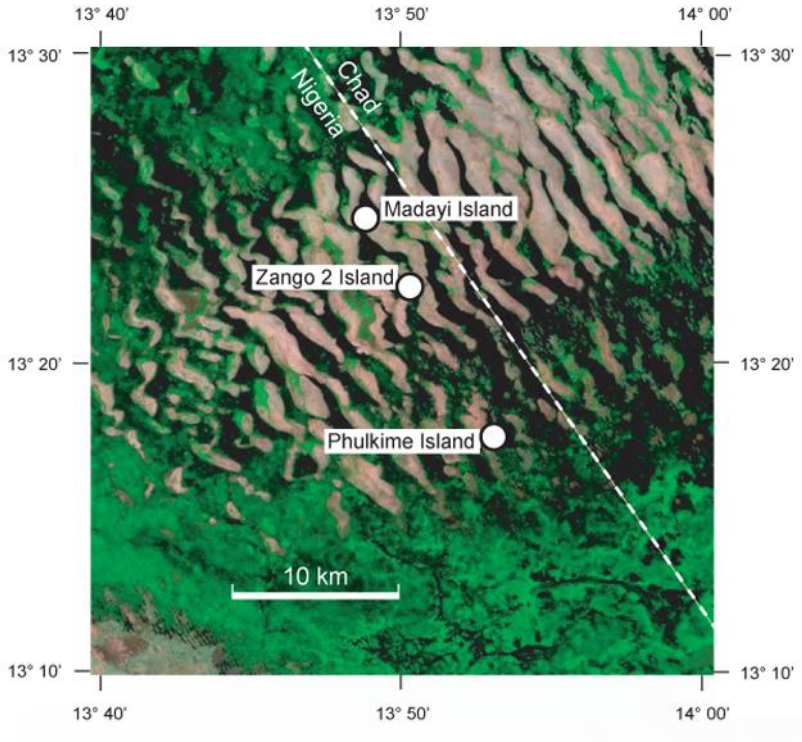

Figure S12. Satellite image of Lake Chad showing NW-SE trending areas of high reflectance (pale grey) that are transverse dunes which were flooded by the rising lake waters at the end of the last ice age, but are now exposed as the lake level has fallen. These dunes are now surrounded by open water (dark areas) and aquatic vegetation (green). The white dots mark the locations of CH33, 34, 35 and 36 on the islands of Phulkime, Madayi and Zango 2.

S4.2 Exhumed dunes in the Bodélé Depression

Partially buried beneath the diatomite of the Bodélé Depression is a field of barchan dunes, which is locally exposed along the southern edge of the depression where the diatomite has been deflated from the tops of the dunes. Subsequent deflation of the sand dunes has created a series of crescentic depressions on the basin floor. These crescentic depressions, each with a low rim of diatomite, are moulds of barchans dunes that were flooded during the lake transgression and buried beneath a layer of diatomite deposited during the lake high-stand. Within the Bodélé, the lake was 160 m deep, and the diatomite deposits are dominated by planctic species *Aulacoseira spp*. The contact between the diatomite and the dune sands is very sharp with no noticeable alteration of the underlying laminated dunes sands or roots (Figure S13). Three exhumed barchan dunes were sampled. In each case, the OSL samples were collected from the downwind margins of the dune where the sand was overlain by diatomite (Figure S13). Sample CH16 was collected from an outcrop close to the campsite at Chicha where fine grained, pale buff coloured, aeolian sand is overlain by around 1m of diatomite. Sample CH22 is from a well exposed section of cross-stratified yellow dune sand overlain by 1.25 m

of diatomite around 29 km downwind from Chicha (Figure S13). Sample CH51 is a further 60 km downwind where pale pink coloured, medium to coarse grained, laminated aeolian sand is overlain by 0.5 m of diatomite.

Figure S13. Outcrop photographs of exhumed dune sample locations: a) CH22 and b) CH51. All locations show a sharp contact between the dune sand and the overlying diatomite with no evidence of soil formation on the dune sand prior to deposition of the diatomite suggesting that the lake level rose rapidly.

The ages of these three exhumed dune samples are remarkably consistent. CH16 and CH22 both have an age of 15.0 ± 1.8 ka, and CH51 has an age of 17.0 ± 2.0 ka. The lack of deformation, reworking, roots, or soil development at the contact between the dune sand and the overlying diatomite, suggests that the change from an arid environment with actively migrating barchans dunes to a lake was extremely fast. We note that the timing of the stabilisation of the dunes in the Bodélé (17.0 ± 2.0 to 15.0 ± 1.8 ka) occurs shortly after the stabilisation of the dune islands in Lake Chad (19.0 ± 2.3 to 15.6 ± 1.9 ka). This is consistent with a northwards migration of the summer rainfall front at the end of the last ice age (27). However, it is equally plausible that the abrupt flooding of the Bodélé dunes occurred when Lake Chad reached the elevation of the Bahr el Ghazal sill (289 ± 1.4 m, 28) allowing surface water to flow into the Bodélé Basin. Thus, the ages of these dunes may represent a threshold response to increased rainfall within the southern hinterland around Lake Chad rather than a northward shift in rainfall to the Bodélé Basin.

S4.3 Mid Holocene reactivated dunes

Two dune samples (BN197, 199) from the Erg du Djourab in the Bodélé Basin, dated by Mauz and Felix-Henningsen (2), are overlain by diatomite. These samples are from their locations 1 and 2 and we have used the SRTM DEM to estimate the elevations of 224 and 265 m respectively (see Section S5). Location 1 is described as “a dune soil complex unconformably overlain by a diatomitic-lacustrine deposit a few decimetres thick” (2, p454) and the dune yielded an OSL age of 4.7 ± 0.2 ka. Location 2 is described as “a sequence of dune sand and diatomitic deposit, overlain by aeolian cover

sand." (2, p454). The OSL sample from location 2 yielded an age of 4.7 ± 0.3 ka. These ages indicate that the Bodélé lake level must have fallen below 224 m significantly before 4.7 ka, to allow time for the hinterland to dry and dunes to become mobilised. These dunes must then have been stabilised around 4.7 ka, and covered by a subsequent rise in lake levels, leading to the deposition of the overlying diatomite.

S4.4 Late Holocene reactivated dunes

Further evidence of dune reactivation is provided by samples from localities 3, 4, and 5 of Mauz and Felix-Henningsen (2). Their location 3 has an OSL age (BN200) of 3.9 ± 0.4 ka. Location 4 has an OSL age (BN201) of 3.4 ± 0.2 ka. Their location 5 has an OSL age (BN202) of 3.1 ± 0.2 ka. Thin soil development is described within the dunes above each sample, which is ascribed to a brief humid period ~ 3ka (2). The flat tops of the "plateau-like dunes" at location 5 (sample BN202) could be taken to indicate that the dunes have been planned-off during a lake transgression, like the dunes around the edge of the Erg du Kanem, where the flattened dunes are interpreted as part of a ravinement surface (1). However, palaeosol development is not consistent with these dunes being flooded. In particular, the Haplic Arenosol at location 5 must have formed above the watertable (2). An alternative hypothesis to explain the flat topped dunes and the palaeosol development is that the dunes at location 5 were deflated down to a level just above the watertable, where the sand was stabilised by vegetation or cohesion in the capillary zone above the water table rather than being completely flooded and mechanically reworked by waves.

S4.5 Beach ridges

Highstand shorelines formed by palaeolake Mega-Chad can be traced almost all the way around the basin, and are expressed as erosional, wave-cut ravinement surfaces, deltas, spits and barrier beaches (1, 28). We have sampled beach ridges from the northern and the southern ends of the basin as well as two of the deltas.

S4.5 The Bama Ridge

The Bama Ridge lies at an elevation of around 339 m in northeastern Nigeria (Figure S3), around 58 m above the present-day level of Lake Chad, and over 165 m above the lowest point in the Bodélé Depression. The ridge is a prominent geomorphological feature in an area with very subdued topography (29). It trends NW-SE and runs diagonally across Northeastern Nigeria from the border with Niger in the north, to the border with Cameroon in the south, a distance of around 330 km. At its northern limits it merges with the edge of the Erg du Kanem which is marked by shorelines that trend NE-SW, with local outcrops of diatomite. At its southern limits a continuing trend can be followed through Cameroon (30). The Bama ridge is a composite feature, with multiple sub-parallel, ridges suggesting that it was formed by several highstands, each of which reached similar elevations. The elevation of the Bama Ridge is thought to be controlled by the Mayo Kebbi sill, which allows Lake Mega-Chad to overflow southwards into the Benue River (28-31).

Two thermoluminescence ages exist for the Bama ridge (4.70 ± 2.85 and 12.6 ± 5.6 ka, 32) exist. These ages have large uncertainties, and thermoluminescence is no longer considered to be the most appropriate method for dating aeolian sand, so we interpret these data as indicating nothing more precise than an early to mid-Holocene age for the Bama Ridge. In this study we sampled the ridge in the suburbs of Maiduguri (Dalori Quarters) and at locations to the northwest of the town (Kurimari and Magumeri) where

the ridge expands forming multiple sub-parallel ridges (Figure S3). OSL samples were collected from aggregate pits in the ridge, which allowed access to sections in fresh exposures, well beneath the weathering zone (Figure S14).

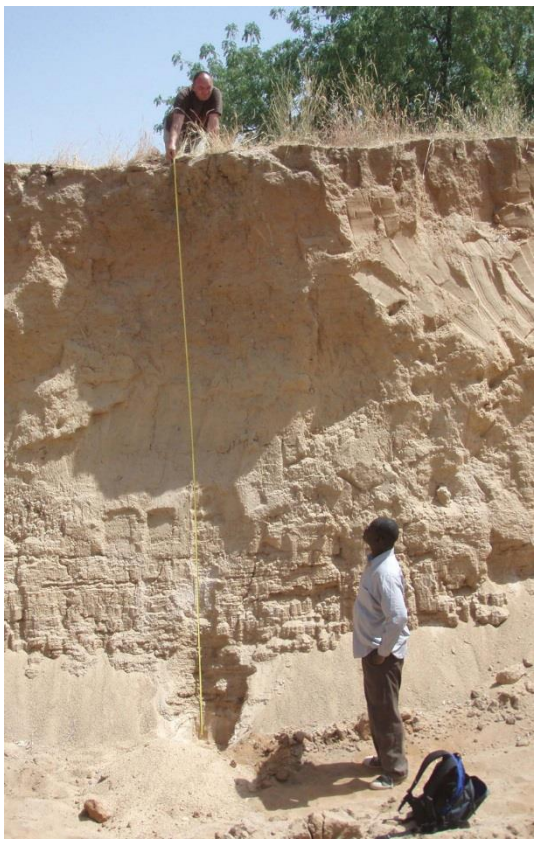

Figure S14. Outcrop photograph of sand pit section Kurimari II. Sample NG11 was taken from this section at a depth of 5 m.

S4.5.1 The Bama Ridge at Dalori Quarters

At Dalori Quarters, on the outskirts of Maiduguri, the Bama Ridge is around 650 m wide, and consists of three low ridges, stepping down from the highest in the southwest to the lowest in the northeast. We excavated four pits in this area, Dalori Quarters 1-4. Dalori Quarters 2-4 form a landward transect, with pit 2 being located in the lowest ridge (nearest to modern Lake Chad) and pit 4 being located on the highest ridge. The Dalori Quarters 1 is located on the lowest ridge, 1.2 km along strike towards the southeast. Sample NG38 (6.5 ± 0.6 ka) was collected from a depth of 1.8 m in well sorted medium to coarse grained beach sand at Dalori Quarters 1. Sample NG39 (6.0 ± 0.6 ka) from Dalori Quarters 2 was collected at a depth of 2.2 m in coarse grained beach sand. Sample NG40 (8.1 ± 0.7 ka) from Dalori Quarters 3 was collected at a depth of 1.7m in coarse to very coarse grained sand, with low-angle stratification and granule layers interpreted as beach deposits. Sample NG41 (19.0 ± 2.0) from Dalori Quarters 4 was collected at a depth of 2.3 m in coarse to very coarse grained sand with cross-strata dipping towards the east. Taken together, these four samples show an increase in age with elevation and distance away from the modern lake Chad, indicating that the elevation of lake high-stands has declined through time. However, while the ages are internally consistent, we regard the age for NG41 (19.0 ± 2.0 ka) as erroneous since: a) it is close to the Last Glacial Maximum, when numerous records indicate extreme aridity (e.g. 23) and b) it is similar to the dates for the dune islands in Lake Chad (samples NG34, 35 and 36) which must have been formed when the lake was dry.

Consequently, while geomorphological and sedimentological evidence from the field support a beach ridge interpretation for sample NG41, the age for this sample has been excluded from our lake level reconstruction.

S4.5.2 The Bama Ridge at Kurimari

At the village of Kurimari, 15 km northwest of the town of Maiduguri the Bama Ridge is around 600 m wide and consists of three low ridges stepping down from the highest in the southwest to the lowest in the northeast. Samples NG9 and NG10 were collected from similar depths in the same sand pit in the lowest of the three ridges, around 70 m apart. Sample NG11 was collected from the second (middle) ridge, 2.5 km along strike towards the northwest. Sample NG9 collected at a depth of 3.5 m was collected from well sorted, coarse to very coarse grained, laminated sand with rare vertical burrows. The laminations dip towards the east at around 10° and the sands are interpreted as beach deposits. Sample NG10 was collected at a depth of 3.4 m from medium to coarse grained sands that coarsen up into coarse then very coarse grained sands and granules. Cross strata within the granules dip at 30° towards the NNE (25°-30°) and are interpreted to be offshore directed bedforms. Sample NG11 was collected from a depth of 5 m in very coarse grained cross-stratified sands (Figure S14). Samples NG9, NG10 and NG11 yield OSL ages of 5.4 ± 0.5, 5.7 ± 0.4, and 9.4 ± 0.9 ka respectively. The two samples from the same ridge (NG9 and NG10) have similar ages with overlapping uncertainties (5.4 ± 0.5 ka, 5.7 ± 0.4 ka) while the middle ridge is older (9.4 ± 0.9 ka). This spatial pattern of ages is similar to that seen at Dalori Quarters, with an increase in age with elevation and distance away from the modern lake Chad.

S4.5.3 The Bama Ridge at Magumeri

Sample NG12 was collected from a road cut section cut through a low ridge exposing medium grained trough cross-stratified sand with gravel lags. Immediately to the north, the Bama Ridge has been cut by an un-named dry river bed. It is unclear whether the outcrop is part of a spit on the south side of the river channel, or part of a river terrace. The cross-strata indicate dune bedforms and northward directed palaeocurrent directions, with palaeoflow towards 340° (n=6). The cross-stratified sands and gravel lags could be interpreted as fluvial channel deposits. However, simulations of surface current (33) indicate westerly flow along this section of the palaeolake shore, which would be consistent with the formation of a spit on the southeast side of a river inlet that crossed the contemporary Bama Ridge shoreline. Sample NG12 yields an OSL age of 8.6 ± 0.7 ka.

S4.6 Ngelewa Ridge

Lower elevation beach ridges within the Chad Basin have been identified (34), including the Ngelewa Ridge (29). The Ngelewa Ridge is oriented northwest – southeast and lies parallel to the Bama Ridge, but at a lower elevation of 295 m estimated from SRTM data (28). The Ngelewa Ridge has been correlated with the elevation of the Bahr el Ghazal sill, indicating that the lake area expands significantly if the water surface exceeds this elevation due to overflow through the Bahr el Ghazal and subsequent flooding of the Bodélé Basin (31). Satellite imagery shows that the Ngelewa Ridge is a composite feature, comprising beach ridges, recurved spits and partially enclosing lagoons. In the field it appears that the topography may have been partly modified by aeolain activity, with small aeolian dunes decorating the crest of the beach ridges. OSL samples were collected from two boreholes on the Ngelwa Ridge. The boreholes were located on the northeast side of the ridge - the side facing Lake

Chad, to avoid sampling aeolian material along the crest and landward side of the ridge. A borehole in a spit at the southern end of the Ngelewa ridge, 6 km north of the village of Kauwa revealed 0.3 m of pale orange coloured sand with traces of charcoal, underlain by fine grained, well sorted, pale orange coloured sand to a depth of 2.3 m. Sample NG29 (2.8 ± 0.2 ka) was collected from a depth of 2.25 m. Two samples from a second borehole on a beach ridge 9 km further north yielded fine and very fine grained, light ochre coloured sands. Samples NG32 and NG31, at depths of 1.75 and 2.95 m, give ages of 3.0 ± 0.2 and 3.2± 0.2 ka respectively.

Ages for the beach ridges and spit at the Ngelewa Ridge are younger than any samples from the Bama Ridge or any of the other high-stand shorelines around palaeolake Mega-Chad. They are slightly younger than the ages of the flat topped plateau-like dunes sampled in the Erg du Djourab (2) and we infer that the shoreline ages correspond with the transgression that flooded the dunes at location 1 and 2 of (2). The Ngelewa Ridge OSL ages presented here are in good agreement with a 3,200 cal. yr BP radiocarbon age for the same feature (35).

S4.7 Northern shores: spits and Cordon Littoral

The most prominent shoreline along the northern shores of Lake Mega-Chad lies above the Falaise de Angamma, an escarpment formed by the Angamma delta and mapped as a cordon littoral (Figure S4, 36). Mapping from satellite imagery (1, 28), shows that the shoreline comprises a barrier beach with a prominent delta as well as spits and cuspate forelands (Figure 3 of 28). At outcrop the cordon littoral is a low ridge capped by well rounded, beach pebbles overlying coarse grained, stratified sands with a heavy mineral lag. Sample CH44 collected from the coarse sands beneath the pebbles of the Cordon Littoral above the delta front has an age of 5.7 ± 0.3 ka. Sample CH46, collected from a beach ridge around 18 km to the east and almost 30 m lower elevation, beneath the delta, has an OSL age of 6.0 ± 0.3 ka.

The eastern shoreline of Lake Mega-Chad is decorated by a series of spits enclosing zeta bays. The spits and embayments have been interpreted as the product of two opposing winds, the north-easterly Harmattan which is dominant during the winter months and the south-westerly summer monsoon (28). Two samples from northeast-soutwest trending beach ridges, on the north side of the prominent spit at Gos Kerki, yield OSL ages of 11.5 ± 0.9 ka and 6.6 ± 0.4 ka (CH74 and CH73 respectively). CH73 is similar in altitude to an intermediate shoreline recognised by Drake and Bristow (2006) and also found at Angamma Delta, Taimanga and South of Goz Kerki with an average height of 322 m. The age of CH73 is consistent with that for the lowest of the dated Bama beach ridges, though its elevation is ~15 m lower, indicating that lake-level fluctuations can occur within the precision of OSL dating. CH74 yielded the earliest Holocene high-stand shoreline age reported in this study (11.5 ± 0.9 ka), and is consistent with the ages for fluvial deposits at Ngomari (Section S4.8).

Regressive, shell-rich, shorelines are reported (1) at a location around 65 km to the north of the Goz Kerki spit described above (16° 24’N 18° 58’E, elevation 325-330 m). Radiocarbon dating of these shells (samples Gif-11510 to 11512) are reported as 3,910 ± 60 (4.52-4.16 cal. ka BP), 4,505 ± 45 (5.31-4.98 cal. ka BP) and 4,510 ± 60 (5.44-4.97 cal. ka BP). These ages postdate our reported high-stand ages and are consistent with an interpretation as regressive shorelines, although they overlap with the widely cited desiccation of the Sahara after 5.5 ka (19). We interpret the youngest age as an

outlier since it is inconsistent with the Erg du Djourab dune reactivation ages (2). Sample GIF11511 and 11512 are younger than our OSL ages for the mid-Holocene highstand, and are here interpreted to indicate that this event ended at ~5 ka.

S4.8 Fluvial deposits

Close to the town of Maiduguri, the River Ngadda (also known as the River Alo) has incised through the Bama Ridge, locally exposing a ~20 m thick section through the underlying sediments. While the surface morphology is one of shore parallel ridges, which we interpret as beach ridges on both morphological and sedimentological grounds (see Section S4.5), the deeper sections exposed in the river valley are revealed as fluvial sediments. A very well exposed section in a sand and gravel pit on the northeast side of the valley close to the village of Ngomari exposes around 6 m of interbedded sand and gravels, capped by a 2 m thick soil (Figure S15). Three samples from this section yield ages 8.2 ± 0.6 ka (NG8, 2.5 m depth), 10.9 ± 0.8 ka (NG7, 6.5 m depth) and 10.4 ± 0.8 ka (NG6, 7.5 m depth). The interbedded sands and gravels are interpreted as shallow sand and gravel braided river deposits with braid bars on the order of 0.5 to 1 m high. Palaeocurrent data from cross-strata at Ngomari indicates that flow was towards the northwest (295° n=14) and that that the Ngadda was flowing parallel to the Bama Ridge on its landward side. The deflection of rivers that flowed towards the palaeolake has been interpreted as resulting from alongshore drift on the Bama Ridge, which deflected the river mouths towards the west (29). Alongshore offset of river mouths and deltas is a common feature of barrier beaches (e.g. 37) and we agree with this interpretation. The location and elevation of the fluvial sediments is consistent with their being deposited by rivers flowing into the palaeolake during a high-stand. Dating of floodplain sediments from the Komadugu- Yobe River (21) suggests that floodplain formation was closely linked to the Holocene oscillations of lake Mega-Chad.

We interpret the Ngomari fluvial deposits as indicative of Lake Mega-Chad highstands. This interpretation is strengthened by the observation that NG6 and NG7 (10.4 ± 0.8 and 10.9 ± 0.8 ka) were deposited close to the time at which the older Goz Kerki beach ridge formed (11.5 ± 0.9 ka, NG74). Similarly, NG8 (8.2 ± 0.6 ka) was deposited during the highstand inferred from the ages for the middle beach ridge at Dalori Quarters and Kurimari. Unfortunately, the Ngomari section was not sampled in sufficient detail to determine whether fluvial deposition at this site was continuous or episodic between 2.5 and 6.5 m, and therefore whether it represents one long high-stand or two shorter ones. However the existence of an as yet undated highest beach ridge at both Dalori Quarters and Kurimari, suggests the existence of a discrete high-stand predating that which occurred between 9.4 and 8.1 ka. Thus we tentatively suggest that samples CH74 (Goz Kerki), NG6 and NG7 (Ngomari) were deposited by a lake high-stand which occurred at 11.5-10.4 ka, and that this high-stand is separate from that which occurred at 9.4-8.1 ka.

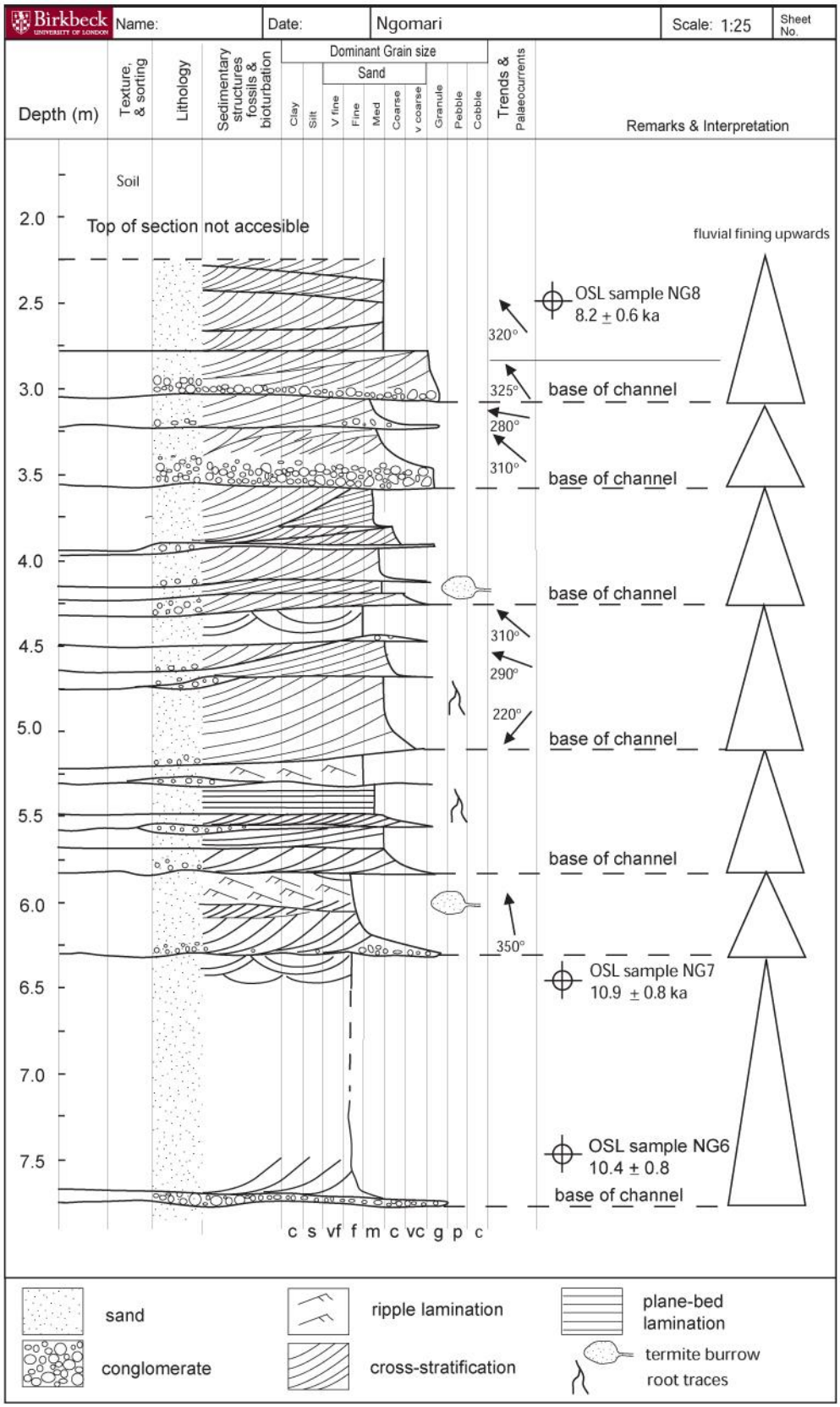

Figure S15. Sedimentary log for quarry sections at Ngomari interpreted as stacked fluvial channel deposits.

S4.9 Deltas

A mesa-like outcrop of pale pink coloured, very fine grained sand overlain by 0.3 m of olive-grey clay, was discovered to the north of the Bahr el Ghazal (3). A sample from this sand (CH62) gave an OSL age of 2.4 ± 0.1 ka. The colour of the clay contrasts with the pale grey to white clays and diatomites commonly found within the Bodélé depression, and XRD analysis indicates that the clay is dominated by kaolinite, which is different form the other clays within the Bodélé. The kaolinite is believed to have been derived from tropical weathering of soils in the southern part of the Chad catchment. The sands and overlying clay are interpreted to be the remains of a delta deposited when the Bahr el Ghazal debouched into the Bodélé, feeding a lake in the base of the depression. The OSL age of 2.4 ± 0.1 ka indicates that water was flowing from Lake Chad in the south to Bodélé and that a lake still stood in the Bodélé around 2.4 ka.

S5 Estimation of the elevation of geomorphic features using remotely sensed data

In this paper we interpret the high-resolution (90 m) SRTM-3 DEM data, acquired by the Spaceborne Imaging Radar-C (SIR-C) radar interferometer (38), processed to remove artefacts in areas of low radar return (39) and converted to Albers equal area projection. The DEM was used to locate and evaluate the elevation landforms in combination with even higher-resolution (30 m) Landsat TM imagery and field visits to the Bodélé Depression in Chad, and the Chad Basin in northern Nigeria.

References

1. Schuster M, *et al.* (2005) Holocene Lake Mega-Chad palaeoshorelines from space. *Quaternary Science Reviews* 24(16-17):1821-1827.
2. Mauz B & Felix-Henningsen P (2005) Palaeosols in Saharan and Sahelian dunes of Chad: Archives of Holocene North African climate changes. *Holocene* 15(3):453-458.
3. Bristow CS, Drake N, & Armitage S (2009) Deflation in the dustiest place on Earth: The Bodele Depression, Chad. *Geomorphology* 105(1-2):50-58.
4. Jacobs Z & Roberts RG (2007) Advances in optically stimulated luminescence dating of individual grains of quartz from archeological deposits. *Evolutionary Anthropology* 16(6):210-223.
5. Wintle AG (2008) Luminescence dating of Quaternary sediments - Introduction. *Boreas* 37(4):469-470.
6. Duller G (2008) *Luminescence Dating: guidelines on using luminescence dating in archaeology* (English Heritage, Swindon).
7. Bøtter-Jensen L, Andersen CE, Duller GAT, & Murray AS (2003) Developments in radiation, stimulation and observation facilities in luminescence measurements. *Radiat Meas* 37(4-5):535-541.
8. Armitage SJ & Bailey RM (2005) The measured dependence of laboratory beta dose rates on sample grain size. *Radiat Meas* 39(2):123-127.
9. Galbraith RF, Roberts RG, Laslett GM, Yoshida H, & Olley JM (1999) Optical dating of single and multiple grains of quartz from Jinmium rock shelter, northern Australia: Part I, experimental design and statistical models. *Archaeometry* 41(2):339-364.
10. Murray AS & Wintle AG (2000) Luminescence dating of quartz using an improved single-aliquot regenerative-dose protocol. *Radiat Meas* 32(1):57-73.

11. Olley JM, Pietsch T, & Roberts RG (2004) Optical dating of Holocene sediments from a variety of geomorphic settings using single grains of quartz. *Geomorphology* 60(3-4):337-358.
12. Duller G (2007) Assessing the error on equivalent dose estimates derived from single aliquot regenerative dose measurements. *Ancient TL* 25:15-24.
13. Duller GAT (2003) Distinguishing quartz and feldspar in single grain luminescence measurements. *Radiat Meas* 37(2):161-165.
14. Adamiec G & Aitken M (1998) Dose-rate conversion factors: update. *Ancient TL* 16(2):37-50.
15. Mejdahl V (1979) Thermoluminescence dating: Beta-dose attenuation in quartz grains. *Archaeometry* 21(1):61-72.
16. Aitken MJ (1985) *Thermoluminescence dating* (Academic press).
17. Prescott JR & Hutton JT (1994) Cosmic ray contributions to dose rates for luminescence and ESR dating: Large depths and long-term time variations. *Radiat Meas* 23(2-3):497-500.
18. Prescott JR & Hutton JT (1988) Cosmic ray and gamma ray dosimetry for TL and ESR. *International Journal of Radiation Applications and Instrumentation. Part* 14(1-2):223-227.
19. deMenocal P, *et al.* (2000) Abrupt onset and termination of the African Humid Period: Rapid climate responses to gradual insolation forcing. *Quaternary Science Reviews* 19(1-5):347-361.
20. Duller GAT (1996) The age of the Koputaroa dunes, southwest North Island, New Zealand. *Palaeogeography, Palaeoclimatology, Palaeoecology* 121(1-2):105-114.
21. Gumnior M & Preusser F (2007) Late Quaternary river development in the southwest Chad Basin: OSL dating of sediment from the Komadugu palaeofloodplain (northeast Nigeria). *Journal of Quaternary Science* 22(7):709-719.
22. Sparks B & Grove A (1964) Fossil non-marine mollusca from Mongonu, NE Nigeria. *Overseas Geology and Mineral Resources* 9:190-195.
23. Weldeab S, Lea DW, Schneider RR, & Andersen N (2007) 155,000 Years of West African monsoon and ocean thermal evolution. *Science* 316(5829):1303-1307.
24. Holmes JA, *et al.* (1999) Holocene landscape evolution of the Manga Grasslands, NE Nigeria: Evidence from palaeolimnology and dune chronology. *Journal of the Geological Society* 156(2):357-368.
25. Grove A & Warren A (1968) Quaternary landforms and climate on the south side of the Sahara. *Geographical Journal* 134:194-208.
26. Clark PU, *et al.* (2009) The Last Glacial Maximum. *Science* 325(5941):710-714.
27. Weldeab S, Frank M, Stichel T, Haley B, & Sangen M (2011) Spatio-temporal evolution of the West African monsoon during the last deglaciation. *Geophysical Research Letters* 38(13).
28. Drake N & Bristow C (2006) Shorelines in the Sahara: Geomorphological evidence for an enhanced monsoon from palaeolake Megachad. *Holocene* 16(6):901-911.
29. Grove AT & Pullan RA (1963) *Some aspects of the Pleistocene palaeogeography of the Chad Basin* (Aldine, Chicago) pp 230-245.

30. Pias J & Guichard E (1957) Origine et conséquences de l'existence d'un cordon sableux dans la partie Sud-Ouest de la cuvette tchadienne. *Comptes Rendus - Geoscience* 244:791-793.
31. Leblanc MJ, *et al.* (2006) Evidence for Megalake Chad, north-central Africa, during the late Quaternary from satellite data. *Palaeogeography, Palaeoclimatology, Palaeoecology* 230(3-4):230-242.
32. Buschbeck HM & Thiemeyer H (1994) Thermoluminescence dating of palaeodunes in northeast Nigeria. *Quaternary Science Reviews* 13(5-7):481-484.
33. Bouchette F, *et al.* (2010) Hydrodynamics in Holocene Lake Mega-Chad. *Quaternary Research* 73(2):226-236.
34. Pias J (1958) Transgression et régressions du lac Tchad à la fin de l'ère Tertiaire et au Quaternaire. *Comptes Rendus de l'Académie des Sciences* 246:800-803.
35. Thiemeyer H (1997) *Untersuchungen zur spätpleistozänen und holozänen Landschaftsentwicklung im südwestlichen Tschadbecken (NE-Nigeria)* (Friedrich-Schiller-Universität Jena, Institut für Geographie).
36. Servant M (1973) Séquences continentales et variations climatiques: Évolution du bassin du Tchad au Cénozoïque supérieur. in *ORSTOM* (Paris), p 348.
37. Hayes MO, Goldsmith V, & Hobbs CH (1970) Offset coastal inlets. *Coastal Engineering Proceedings* 1(12).
38. Rabus B, Eineder M, Roth A, & Bamler R (2003) The shuttle radar topography mission - A new class of digital elevation models acquired by spaceborne radar. *ISPRS Journal of Photogrammetry and Remote Sensing* 57(4):241-262.
39. Jarvis A, Rubiano J, Nelson A, Farrow A, & Mulligan M (2004) Practical use of SRTM data in the tropics–comparisons with digital elevation models generated from cartographic data. in *Working document no. 198* (International Centre for Tropical Agriculture (CIAT)).